Available online at www.sciencedirect.com
ScienceDirect
Journal of Catalysis 250 (2007) 67–74
JOURNAL OF CATALYSIS
www.elsevier.com/locate/jcat

Generation of hydrogen and light hydrocarbons for automotive exhaust gas purification: Conversion of *n*-hexane in a PACT (plasma and catalysis integrated technologies) reactor

Yu Xing [a], Zhenxin Liu [a], Richard A. Couttenye [b,1], William S. Willis [a], Steven L. Suib [a,b,*], Paul T. Fanson [c], Hirohito Hirata [d], Masaya Ibe [d]

[a] *Department of Chemistry, University of Connecticut, Storrs, CT 06269-3060, USA*
[b] *Department of Chemical, Materials & Biomolecular Engineering, University of Connecticut, Storrs, CT 06269-3060, USA*
[c] *Toyota Motor Engineering and Manufacturing North America, Inc., Ann Arbor, MI 48105, USA*
[d] *Toyota Motor Company, Japan, 1 Toyota-cho, Toyota, Aichi, 471-8572, Japan*

Received 26 March 2007; revised 22 May 2007; accepted 22 May 2007

Available online 29 June 2007

Abstract

Conversion of a model hydrocarbon (*n*-hexane) was carried out over iron and nickel electrodes in an alternating current (AC) discharge plasma and catalysis integrated technologies (PACT) reactor to instantly produce hydrogen and light alkanes and alkenes, at room temperature and atmospheric pressure, for possible application in automotive exhaust gas purification. Catalytic effects of metal electrodes are involved in the reactions, with iron electrodes showing obviously higher catalytic activity on addition reactions compared with nickel electrodes. Cracking of carbon–carbon bonds is the dominant reaction. Catalytic dehydrogenation of hexane is the source of hydrogen. Compared with space velocity, applied voltage has dominant effects on power consumption. Energy efficiency will increase as the residence time of feed molecules decreases and decrease as applied voltage increases. A maximum of 38% of the energy consumed by the PACT reactor was used for cracking single carbon–carbon bonds.

Keywords: Automotive exhaust gas; Nonthermal plasma; NO_x storage-reduction; Catalytic dehydrogenation; Hydrogen generation; Hydrocarbon cracking

1. Introduction

Improvements in health, environmental, and ecological conditions requires increasingly stringent emission regulations, including limits on NO_x, CO, and hydrocarbon emissions from vehicle engines. Greenhouse gas emissions, such as CO_2, are also under increasing scrutiny, as is the need to increase engine fuel economy [1]. One way to reduce CO_2 emissions while simultaneously improving overall fuel economy is through the use of lean-burn gasoline and diesel engines; however, this produces oxygen-rich exhaust gases [1–3]. Removing NO_x from oxygen-rich exhaust gases with conventional three-way catalysts has proven to be extremely difficult. This situation has prompted research into the development of a new catalyst technology called NO_x storage-reduction (NSR) catalysis, which is operated cyclically and is capable of selectively storing NO_x under lean conditions and then nonselectively reducing the stored NO_x under short, rich (reducing) pulses [1,3]. The regenerating rich pulse is typically accomplished by engine control or by direct injection of diesel fuel into the exhaust stream. However, the long-chain hydrocarbon molecules found in automotive fuel typically have very low reactivity. Much higher NO_x reduction efficiency could be achieved if the hydrocarbon fuel could be first cracked on board to a lighter hydrocarbon, such as ethylene (C_2H_4), propylene (C_3H_6), or H_2. In addition, light hydrocarbons and H_2 are also more reactive for the regeneration of sulfur-poisoned NO_x storage catalysts [1,3,4]. Our

* Corresponding author. Fax: +1 860 486 2981.
E-mail address: steven.suib@uconn.edu (S.L. Suib).
[1] Present address: Kraft Foods R&D Center, 801 Waukegan Road, Glenview, IL 60025, USA.

0021-9517/$ – see front matter
doi:10.1016/j.jcat.2007.05.021

group showed previously that microwave energy can be used to remove sulfur from a poisoned NSR catalyst at very low temperature (200 °C) in the presence of a reducing agent, such as hydrogen [5].

Traditional hydrocarbon-cracking technologies [6] are not suitable for on-board automotive systems because of the need for catalyst warm-up time, a hydrogen source, or coke removal. A possible alternative strategy is to use nonthermal plasma technology, which has received considerable attention in the fields of chemistry and material processing [7]. In addition, catalysis technology has been successfully combined with nonthermal plasma technology in various applications [8–13].

Herein we report a method for instantly generating hydrogen and light hydrocarbons, such as alkanes and alkenes, at low temperature and atmospheric pressure, for automotive NO_x storage-reduction (NSR) catalytic systems. This method is achieved by converting long-chain hydrocarbons in a plasma and catalysis integrated technologies (PACT) reactor with an iron or nickel electrode. Here *n*-hexane was used as the model hydrocarbon.

2. Experimental

2.1. PACT tubular reactor setup

The reactions were carried out in a PACT tubular reactor with interchangeable electrodes (Fig. 1), comprising an exchangeable, cylindrical, nonporous inner metal electrode (10 cm long, 8 mm i.d.), screwed onto a supporting metal rod, and a quartz tube (17.9 cm long, 9.85 mm i.d., 12.55 mm o.d.) acting as a dielectric separating outer and inner electrodes. Aluminum foil (10 cm long) is wrapped around this outer electrode.

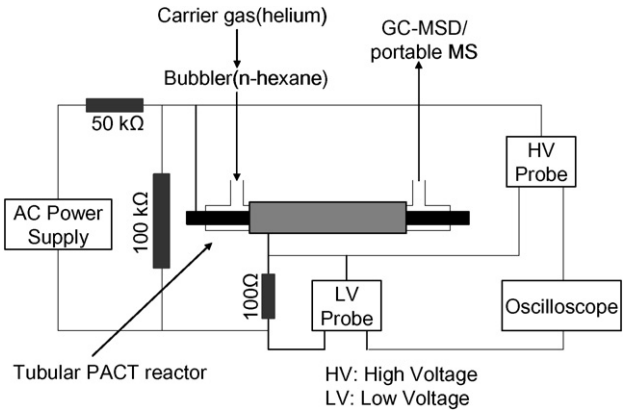

Fig. 1. Schematic diagram of the experimental setup for plasma generation and monitoring voltage and current conditions.

The exchangeable electrode consists of the electrode itself and a metal rod onto which this electrode is screwed. Various materials, such as iron and nickel, were electroplated onto a copper rod at a thickness of 100 μm; these products were used as electrodes. The exposed end of the supporting metal rod was used as the electrical contact for the inner metal electrode to the high-voltage alternating current (AC) power source. The metal electrodes were obtained from Mitsubishi Materials Corporation. Table 1 shows detailed data on the types of the electrodes used in this research and the sizes of plasma zones. The iron (Fe) and nickel (Ni) electrodes used in this research were the same shape and size.

2.2. Circuit setup

The circuit setup is also shown in Fig. 1. The high-voltage supply was 120 V AC (60 Hz), with the high voltage generated by an UHV-10 AC high-voltage power supply. A digital DL-1540 Yokogawa oscilloscope with a high-voltage probe (Tektronix P6025) and a low-voltage probe (Yokogawa 70996) was used to measure input voltage and input current of the PACT reactor. The voltage across a 100-Ω standard resistor in series with the reactor was used to determine the input current.

2.3. Experimental parameters and product analysis

In a typical experiment, carrier gas (helium) was passed through a bubbler containing about 500 mL of *n*-hexane liquid at a flow rate of 44 mL/min under the control of an Aalborg mass flow controller, and the gaseous mixture was introduced into the PACT reactor at room temperature and atmospheric pressure. Hexane, purchased from J.T. Baker, contained 95% *n*-hexane and 5% hexanes, including methyl cyclopentane and 3-methyl pentane. The reactor's inner metal electrode, made of iron (Fe) or nickel (Ni), was connected to the high-voltage line, whereas the outer aluminum/quartz electrode was connected to the ground line.

During the experiments, the PACT reactor was not heated, and no significant temperature change was observed. For the purpose of simplification, the reactor was assumed to be an ideal plug flow reactor. The reaction system was vented to atmosphere, which maintained a constant reactor pressure at atmospheric pressure. The set carrier gas flow rate under these experimental conditions was 15, 44, 87, 145, or 218 mL/min. Due to the use of the dial of the UHV-10 HV supply and the consistency of tests, the set value of applied voltage under these experimental conditions was 5.4, 6.8, 8.2, 9.5, 10.6, or 12.0 kV. Unless specified otherwise, the reactor was run for 20 min to

Table 1
Plasma zone data for iron (Fe) and nickel (Ni) electrodes installed in the PACT reactor

Inner electrode	Inner electrode diameter (cm)	Electrode length (cm)	Electrode surface area in plasma zone (cm^2)	Diameter of inner wall of quartz tube barrier (cm)	Gap size[a] (mm)	Plasma zone volume[b] (cm^3)
Fe or Ni	0.800	10.000	25.130	0.985	0.925	2.594

[a] The distance between the surface of inner metal electrode and the inner wall of tubular quartz barrier.
[b] The volume of the cavity between the inner metal electrode and the inner wall of quartz tube of the outer electrode, where a non-thermal plasma be generated by AC discharge and exists.

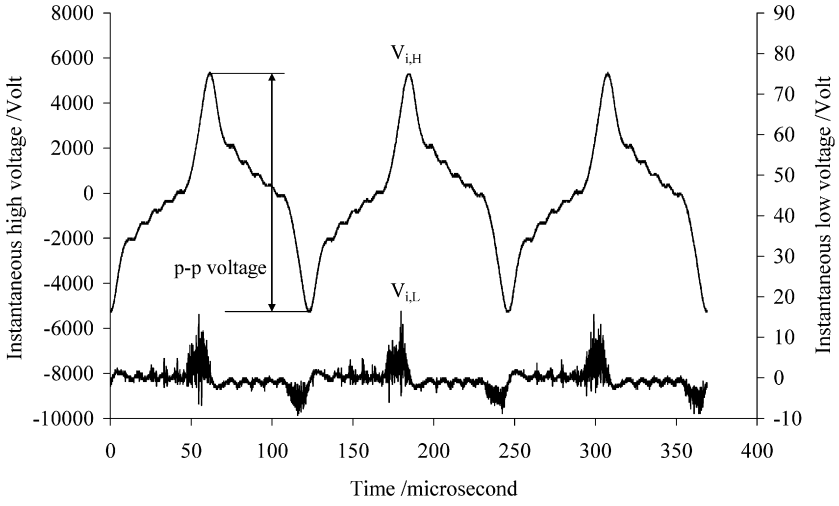

Fig. 2. Instantaneous high voltage ($V_{i,H}$) and instantaneous low voltage ($V_{i,L}$) measured by digital oscilloscope.

allow the system to come to equilibrium before an effluent gas sample was collected.

Gas chromatography–mass spectroscopy (GC–MS) was used for identification and quantification of product mixtures. During each 20-min test, the amount of coke produced was negligible and was not counted in the calculation of yield data. The reaction mixture in the outlet of the PACT reactor was monitored continuously with a portable MKS-UTI MSS quadrupole residual gas analyzer mass spectrometer. Samples from the outlet gaseous stream were analyzed using a Hewlett Packard 5970 series mass selective detector coupled to a Hewlett Packard 5890 gas chromatograph equipped with a thermal conductivity detector and a SUPELCO PETROCOLTM DH150 capillary column (150 m long, 0.25 mm diameter, 1.0 μm film thickness), which is commonly used for the analysis of refinery gases, including methane.

2.4. Determination of power consumption and power efficiency

The instantaneous power (P_i) delivered to a load can be expressed as

$$P_i = V_i \times I_i, \quad (1)$$

where V_i is the instantaneous voltage and I_i is the instantaneous current. Here V_i is the instantaneous high voltage ($V_{i,H}$) applied to the PACT reactor, which can be measured directly by the oscilloscope with high-voltage probes. The I_i equals the current through the 100-Ω standard resistor. The voltage of the standard resistor, instantaneous low voltage ($V_{i,L}$), can be measured directly by the oscilloscope with low-voltage probes. Therefore, I_i can be obtained using Ohm's law. Fig. 2 shows the $V_{i,H}$ and $V_{i,L}$ measured by a digital oscilloscope. The values of $V_{i,H}$ and $V_{i,L}$ are used to calculate the average power (P_{avg}), the net average power consumed by the PACT reactor, which is used to determine the energy efficiency, defined here as the amount of the feed converted or the products yielded per J of electrical energy consumed.

Table 2
Feed supply, space velocity, and residence time of feed molecules at different flow rates of carrier gas helium

Flow rate of carrier gas helium (mL/min)	Hexane supply rate (g/h)	Hexane-based space velocity (h^{-1})	Residence time of feed molecules (s)
15	0.618	68	8.91
44	3.370	369	2.61
87	4.773	522	1.42
145	6.190	677	0.89
218	9.446	1033	0.59

3. Results and discussion

3.1. Conversion of n-hexane at different carrier gas flow rates

Table 2 shows that hexane supply rate (i.e., the amount of hexane carried away by helium from the bubbler per hour), increased rapidly with increasing carrier gas flow rate. Hexane-based space velocity (SV), as shown in Table 2, is defined here as volumetric flow rate of gaseous hexane through the reactor divided by the volume of the plasma zone of the reactor. This SV has the same trend as the hexane supply rate. Residence time denotes the average time it takes for individual gaseous hexane molecules to pass through the plasma zone with a length of 10 cm. As the helium flow rate decreased from 218 to 44 mL/min, the residence time of hexane molecules in the plasma zone increased slowly from 0.59 to 2.61 s. As the helium flow rate decreased from 44 to 15 mL/min, the residence time increased sharply from 2.61 to 8.91 s.

As shown in Fig. 3, as the helium flow rate increased from 15 to 218 mL/min, the conversion rapidly decreased for both iron and nickel electrodes. This is consistent with the data for residence time of feed molecules shown in Table 2. At the same applied p–p voltage, the longer the residence time of the feed molecules, the higher the conversion that could be obtained. At every flow rate, under a constant p–p voltage of 10.6 kV, the conversion over the iron electrode was higher than that over the

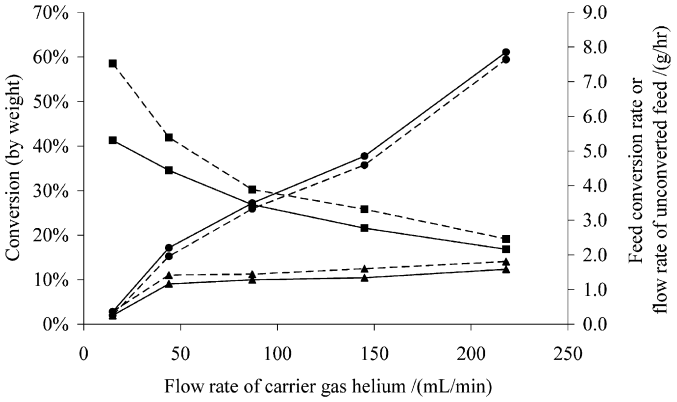

Fig. 3. Conversion vs flow rate of carrier gas helium (applied p–p voltage: 10.6 kV; (■) conversion; (▲) feed conversion rate; (●) flow rate of unconverted feed; (—) Ni electrode; (- - -) Fe electrode).

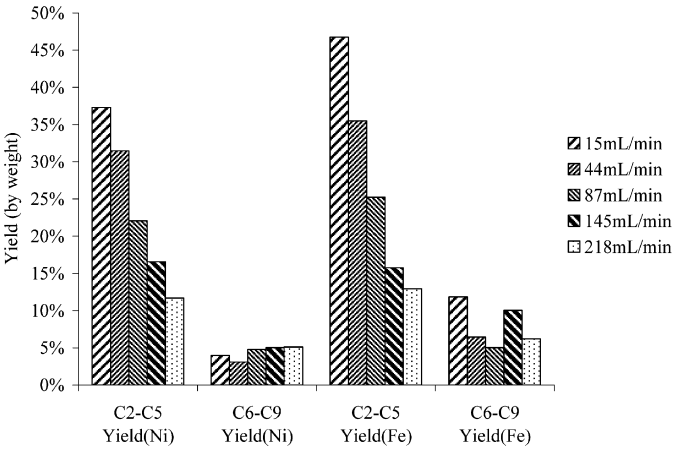

Fig. 4. Yield vs flow rate of carrier gas helium (applied p–p voltage: 10.6 kV).

nickel electrode. For a p–p voltage of 10.64 kV, the maximum conversion observed (at 15 mL/min helium flow) was almost 60% for the iron electrode, compared with only slightly above 40% for the nickel electrode. These findings verify that iron electrodes are more reactive than nickel electrodes under these conditions. The feed conversion rates (defined as the amount of hydrocarbon feed converted per hour) of both the iron and nickel electrodes increased rapidly as the helium flow rate was increased from 15 to 44 mL/min, and then increased slowly as the helium flow rate was increased from 44 to 218 mL/min. However, as shown in Table 2, the hexane supply rate increased rapidly with increasing carrier gas flow rate. The final result is that the amount of unconverted hexane feed increased rapidly as the helium flow rate was increased, as shown in Fig. 3. Having considerable unconverted hexane feed for the NSR catalytic system is unfavorable; therefore, the design of the reactor system must be optimized, with careful consideration given to the flow rate.

Considering the data in Fig. 3 and Table 2 reveals that the conversion of both iron and nickel electrodes increased rapidly as the residence time of hexane molecules was increased from 0.59 to 2.61 s, and then increased slowly as this residence time was increased from 2.61 to 8.91 s. This indicates that overly

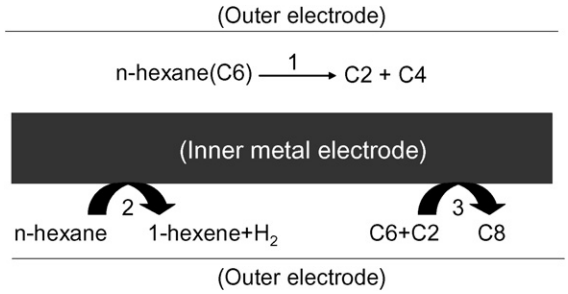

Fig. 5. Schematic diagram of some reactions in the PACT reactor. 1, noncatalytic cracking reaction in the gaseous phase. 2, catalytic dehydrogenation on the surface of metal electrode. 3, catalytic addition on the surface of metal electrode.

high residence times of hexane molecules (e.g., 8.91 s) are not favored, because conversion did not increase significantly as the hexane supply rate was decreased, which can finally cause the feed conversion rate to be very low.

Fig. 4 shows the effect of electrode composition and flow rate on the product distribution observed in this reaction. The term C_2 denotes the hydrocarbons, such as ethane and ethylene, which have two carbon atoms in each molecule. The terms C_3, C_4, and so on are defined similarly. Fig. 4 shows that for both the iron and nickel electrodes, the total yield of C_2–C_5 products was obviously higher than that of C_6–C_9 products. This verifies that cracking was the major reaction, whereas the other reactions were all minor reactions. Fig. 4 also indicates that a longer residence time of hexane molecules will facilitate cracking reactions rather than other types of reactions. Iron electrodes produced considerably more unfavorable C_6–C_9 products than nickel electrodes.

Fig. 4 also shows that for both iron and nickel electrodes, the total yield of favored C_2–C_5 products decreased rapidly as the helium flow rate was increased from 15 to 218 mL/min, whereas the total yield of unfavorable C_6–C_9 products remained fairly constant as plotted versus the flow rate of carrier gas. This indicates that cracking reactions that produce C_2–C_5 products may have occurred primarily in the gas phase of the plasma zone rather than on the electrode surface, whereas the reactions to make C_6 and larger molecules seemed unaffected by the flow rate of carrier gas and thus may be have occurred on the electrode surface rather than in the gas phase. The reaction schematic is shown in Fig. 5. Because the surface of the metal electrode is not involved, the cracking reactions in the gas phase are noncatalytic reactions and are dominated by the plasma, such as the residence time in plasma zone. The reactions on the electrode surface are basically catalytic reactions, because the surface of the metal electrode (i.e., the catalyst) may be involved in the absorption of feed molecules (or radicals/ions), formation of intermediates and products, and desorption of products. Once these interface processes reach an equilibrium, the catalytic reactions on electrode surface will be unaffected by the concentration of feed molecules in the gas phase, which is controlled by the flow rate of carrier gas.

The C_6 products are mainly hexenes from the dehydrogenation of hexane, with some hexane isomers from the isomerization of hexane. The C_7–C_9 products are possibly part of the

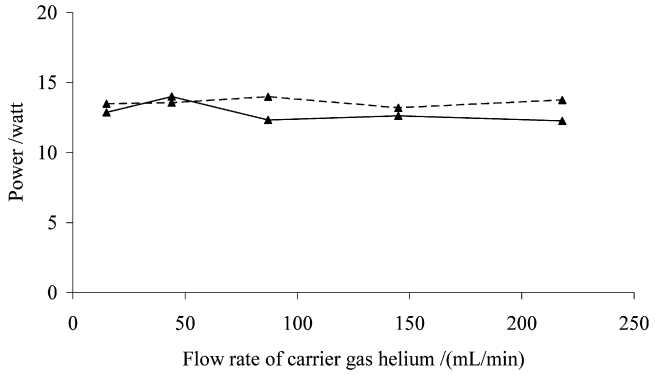

Fig. 6. Power vs flow rate of carrier gas helium (applied p–p voltage: 10.6 kV; (▲) $P_{(avg)}$; (—) Ni electrode; (- - -) Fe electrode).

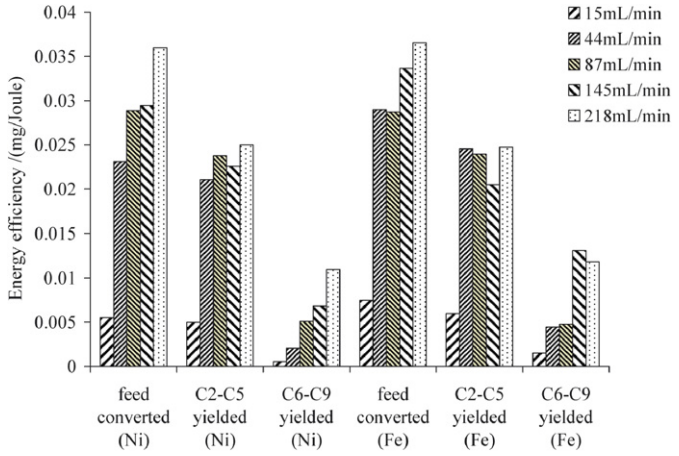

Fig. 7. Energy efficiency vs flow rate of carrier gas helium (applied p–p voltage: 10.6 kV).

products of disproportionation reactions, such as the reaction between two C_6 hydrocarbon (HC) molecules to form one C_4 HC molecule and one C_8 HC molecule. The mechanism of the these disproportionation reactions under plasma conditions remains unclear, but the cracking of single carbon–carbon bonds and the recombination of produced fragments (e.g., radicals, hydride ions, carbocations, and/or carbanions) are purportedly involved in the formation of C_7–C_9 products. Free radical addition and electrophilic addition onto carbon–carbon double bonds are highly possible pathways for the formation of C_7–C_9 products in plasma conditions.

Fig. 6 shows that for both iron and nickel electrodes, the average power values underwent no considerable changes as the helium flow rate changed from 15 to 218 mL/min. This verifies that the carrier gas flow rate, which caused obvious differences in hexane-based space velocity, had a very limited effect on average power consumption.

Fig. 7 shows that for both iron and nickel electrodes, the energy efficiencies for feed conversion, for yields of favored C_2–C_5 products, and for yields of unfavorable C_6–C_9 products all had their minimum values at the lowest helium flow rate of 15 mL/min, and all increased as the helium flow rate changed from 15 to 218 mL/min. This indicates that overly high residence times of hexane molecules (e.g., 8.91 s) will

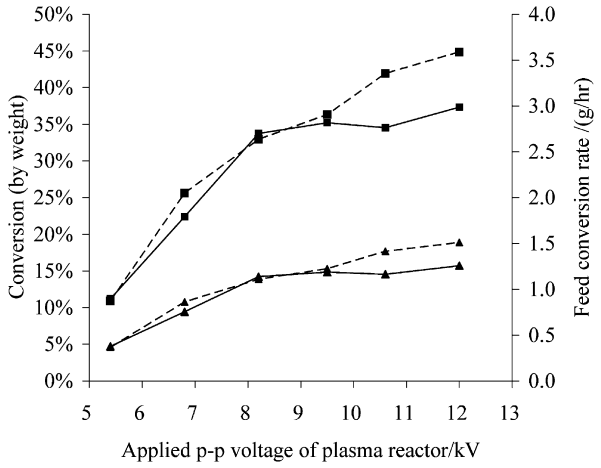

Fig. 8. Conversion vs applied p–p voltage (flow rate of carrier gas helium: 44 mL/min; (■) conversion; (▲) feed conversion rate; (—) Ni electrode; (- - -) Fe electrode).

waste considerable electrical energy and greatly decrease the energy efficiency. This further supports the finding that within the set values, 44 mL/min is the optimal carrier gas flow rate for this PACT reactor, at which high conversion, high favored C_2–C_5 yield, low unfavorable C_6–C_9 yield, and satisfactory energy efficiency can be achieved.

3.2. Conversion of n-hexane at different applied peak-to-peak (p–p) voltages

Fig. 8 shows that for both iron and nickel electrodes, conversion increased as the applied p–p voltage increased from 5.4 to 12.0 kV. The conversions over iron and nickel electrodes were close in a low p–p voltage range of 5.4–9.5 kV and diverged in a high p–p voltage range above 9.5 kV. At high p–p voltage above 9.5 kV, the conversion over iron electrodes increased rapidly and became obviously higher than that over nickel electrodes. This indicates that the activity of iron and nickel electrodes were close in a low p–p voltage range of 5.4–9.5 kV and became different in a high p–p voltage range above 9.5 kV. The feed conversion rates are a function only of conversion; the space velocities remain constant. Therefore, feed conversion rates showed the same trends as conversion.

No reactions occurred at applied p–p voltages below 5.4 kV. This explains the relationship between the plasma reactor and the catalyst. The catalyst itself (i.e., the metal electrode) cannot catalyze any hydrocarbon reactions at room temperature due to the existence of an energy barrier, which must be overcome for activation of the molecules. The function of the plasma reactor is to provide electrical energy rather than thermal energy to activate the molecules at room temperature and also to sustain the plasma status through continuously supplying AC discharge to the plasma zone. Once plasma is generated, feed molecules will be ionized and may be converted into products spontaneously (i.e., noncatalytically) or catalytically. Catalysts like the inner metal electrode of a PACT reactor then can function in

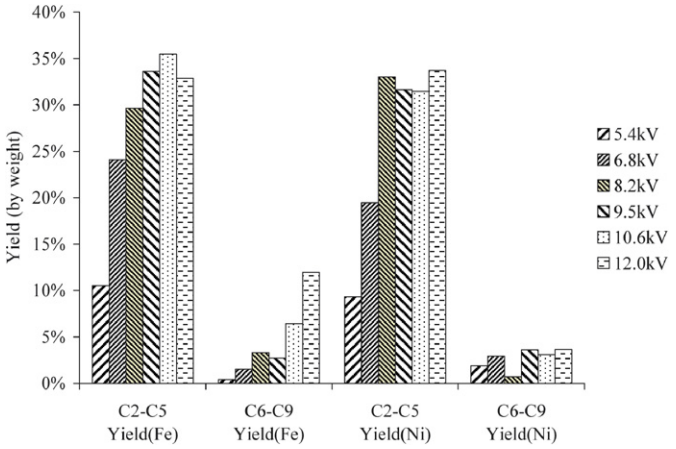

Fig. 9. Yield vs applied p–p voltage (flow rate of carrier gas helium: 44 mL/min).

plasma zones to introduce the ionized species into special reaction pathways and produce products with special selectivities.

Fig. 9 shows that for both iron and nickel electrodes, increasing the voltage caused an initial sharp rise in the yields of favored C_2–C_5 products that nearly leveled off at 8.2 kV. As the applied p–p voltage was increased from 5.4 to 12.0 kV, the total yield of unfavorable C_6–C_9 products over nickel electrodes showed a slowly increasing trend, whereas the total yield of unfavorable C_6–C_9 products over iron electrodes showed a rapidly increasing trend. At high p–p voltage above 9.5 kV, total yield of unfavorable C_6–C_9 products over iron electrodes became obviously higher than that over nickel electrodes. This finding suggests that iron electrodes had obviously higher catalytic activity for addition reactions than nickel electrodes. It also indicates that the performance of the iron and nickel electrodes were close in a low p–p voltage range of 5.4–9.5 kV and became different in a high p–p voltage range above 9.5 kV. Consequently, nickel electrodes are preferred to iron electrodes for operation at high p–p voltages above 9.5 kV, because nickel electrodes produce unfavorable C_6–C_9 products with lower yield. Nickel electrodes can be used in a wider p–p voltage range than iron electrodes. Figs. 4 and 9 show that those reactions, which occur on the electrode surface and are catalyzed by the electrode surface to produce C_6 and larger molecules, are obviously affected by applied voltage but seem unaffected by the flow rate of carrier gas. Figs. 4 and 9 also show that the cracking reactions, which occur primarily and noncatalytically in the gas phase, are obviously affected by both the applied voltage and the flow rate of carrier gas.

Fig. 10 shows the yield changes of individual components from C_2 to C_9 as the p–p voltage changed from 5.4 to 12.0 kV. For both iron and nickel electrodes, the reactions produced mostly C_3, with large amounts of C_2 and C_4 as well. The distributions of C_2, C_3, C_4, and C_5 products for iron and nickel electrodes were very similar in iron and nickel electrodes, whereas the distributions of C_6, C_7, C_8 and C_9 products differed.

The absolute average power values increased as the applied p–p voltage was increased from 5.4 to 12.0 kV, as shown in Fig. 11. The data in Figs. 6 and 11 demonstrate that power consumption of a PACT reactor is dominated by applied p–p voltage but is not obviously effected by feed supply rate or space velocity. The power consumption of iron and nickel electrodes at different p–p voltages was very similar.

Fig. 12 shows that except for the energy efficiency for yields of unfavorable C_6–C_9 products over iron electrodes, the energy efficiency for converting the feed, for yields of favored C_2–C_5 products, and for yields of unfavorable C_6–C_9 products all had maximum values at the lowest p–p voltage of 5.4 kV. Moreover, all showed a decreasing trend as the p–p voltage changed from 5.4 to 12.0 kV for both iron and nickel electrodes.

The tabulated bond energy of single carbon–carbon bonds was about 347 kJ/mol; thus, the theoretical maximum energy efficiency for cracking carbon–carbon bonds is about 2.882E−03 mol/kJ (= 1/(347 kJ/mol)). The highest energy efficiency achieved by the nickel electrode was 0.0946 mg/J, which

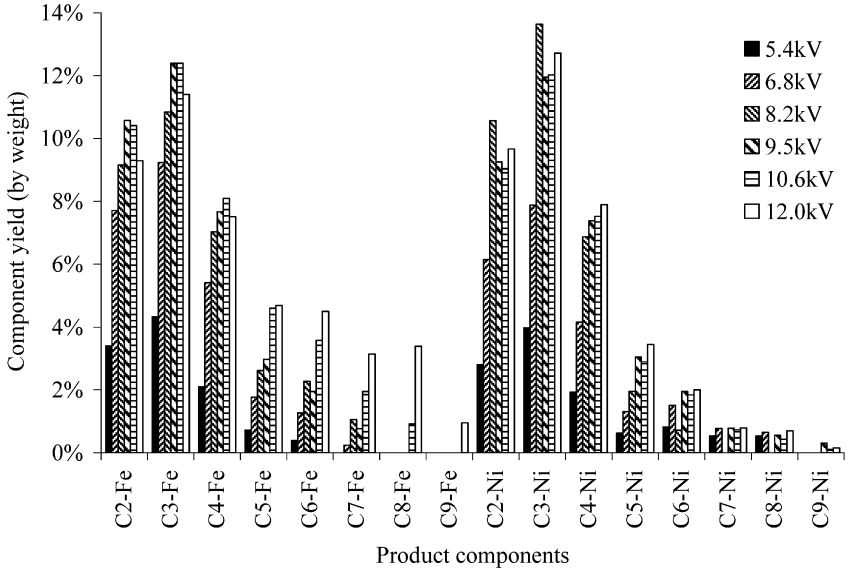

Fig. 10. Yields of product components at different applied p–p voltages (flow rate of carrier gas helium: 44 mL/min).

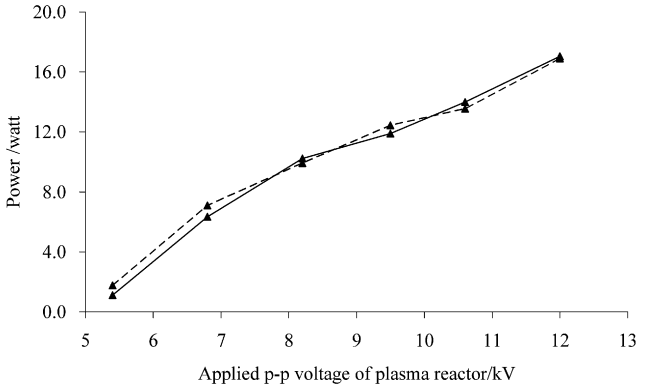

Fig. 11. Power vs applied p–p voltage (flow rate of carrier gas helium: 44 mL/min; (▲) $P_{(avg)}$; (—) Ni electrode; (- - -) Fe electrode).

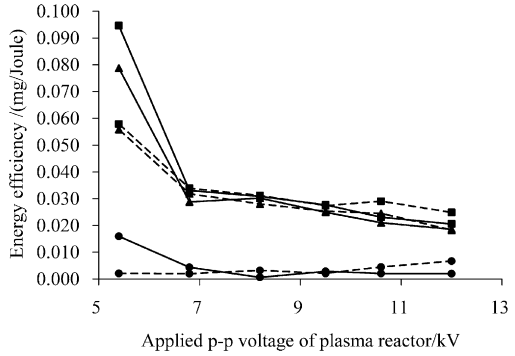

Fig. 12. Energy efficiency vs applied p–p voltage (flow rate of carrier gas helium: 44 mL/min; (■) feed converted; (▲) C_2–C_5 yielded; (●) C_6–C_9 yielded; (—) Ni electrode; (- - -) Fe electrode).

equals 1.098E−03 mol/kJ. The ratio of this practical energy efficiency to the theoretical maximum energy efficiency is 38%. This means that a maximum of 38% of the energy consumed by the PACT reactor was used for cracking carbon–carbon bonds.

3.3. Detection of hydrogen and methane by online mass spectrometry

A 150-m-long PETROCOL DH150 capillary column was installed in the gas chromatograph–mass spectrometer, which can detect light hydrocarbons, including methane. However, no methane peaks were observed through GC–MS analysis. The detection of methane had to be done using a portable MKS-UTI MSS quadrupole residual gas analyzer mass spectrometer, which has a higher sensitivity for even trace chemicals.

Fig. 13 shows part of the signals obtained during online mass spectrometry studies. The total pressure originally detected was not constant but varied; thus, the signals of a component cannot be directly used for comparison. Assuming that total pressure is a constant value, calculation of the partial pressures of components is necessary for effective data comparisons. All data shown in Fig. 13 were precalculated based on an assumed constant total pressure of 9.80E−06 Torr. The gradual decrease in the partial pressure of helium ($m/z = 4$) was due to the gradual increase of total molar number in the gaseous stream caused by cracking reactions. Methane is detected with a slowly in-

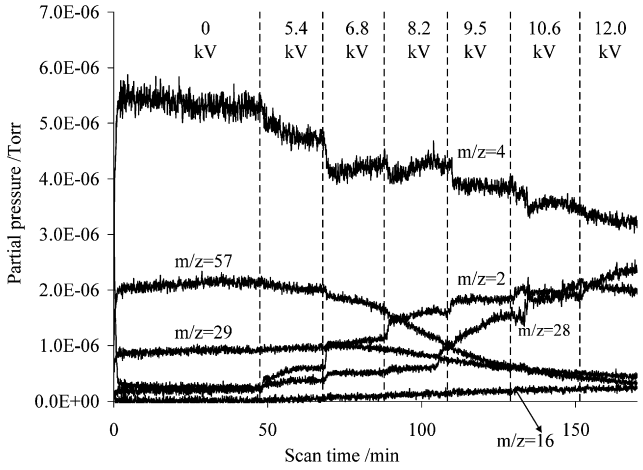

Fig. 13. Online mass spectrometry studies of hexane conversion over nickel electrode (partial pressure: calculated by assuming a constant total pressure of 9.80E−06 Torr; flow rate of carrier gas helium: 44 mL/min).

creasing trend. The partial pressure of methane ($m/z = 16$) was far below the partial pressure of hydrogen, a product of a minor reaction (i.e., dehydrogenation). Another signal of methane ($m/z = 15$) almost overlapped with the signal of $m/z = 16$ and thus is not given in Fig. 13. These data verify that methane was surely produced but at very low concentrations (<1%) during hexane conversion in the PACT reactor. The low methane concentration and the relatively high C_5 concentration indicate that the amount of C_1 intermediates formed by the breaking of single α-carbon–carbon bonds of hexane might exceed the amount of methane and could be combined with other active intermediates in the plasma zone to form new hydrocarbons, such as C_7–C_9. Methane is not favored due to its high chemical stability and consequent poor consumption during steam reforming.

Fig. 13 also shows that reactions began immediately after the voltage was applied to the PACT reactor, which can produce hydrogen and light hydrocarbons instantly at room temperature and atmospheric pressure. The partial pressure of hydrogen increased stepwise as the applied p–p voltage was increased stepwise from 5.4 to 12.0 kV. The output of hydrogen generated during hexane conversion over the nickel electrode increased from 0.60 to 3.90 mL/min as the applied p–p voltage was increased from 5.4 to 12.0 kV. Once a hexane/helium plasma was generated at an applied p–p voltage of 5.4 kV, hydrogen was produced immediately. Once the applied p–p voltage was turned off after a high value of 12.0 kV, the partial pressure of hydrogen dropped immediately, and then quickly disappeared. Analysis of product components determined by GC–MS shows that catalytic dehydrogenation of hexane was the source of hydrogen and hexenes.

4. Conclusion

Conversion of a model hydrocarbon (n-hexane) in a PACT reactor has been verified to be an effective method to instantly produce hydrogen and light hydrocarbons, such as alkanes and alkenes, at room temperature and atmospheric pressure for automotive exhaust gas purification. Cracking of carbon–carbon

bonds is the dominant reaction during *n*-hexane conversion. Cracking reactions, which produce C_2–C_5 products and may occur primarily in the gas phase of the plasma zone, are possibly noncatalytic reactions and are obviously affected by both the applied voltage and the flow rate of carrier gas. The reactions, which make C_6 and larger molecules and may occur on the electrode surface, are basically catalytic reactions and are obviously affected by applied voltage, but seem to be unaffected by the flow rate of the carrier gas. Conversion is affected mainly by the electrode material, applied voltage, and residence time of feed molecules. Effects of carrier gas flow rate, which controls the space velocity and the residence time of feed molecules, were studied, and an optimal value within set values was found. Iron and nickel electrodes demonstrated similar performance in a low p–p voltage range of 5.4–9.5 kV but became different in a high p–p voltage range above 9.5 kV. Iron electrodes showed obviously higher catalytic activity for addition reactions compared with nickel electrodes. Compared with iron electrodes, nickel electrodes produce unfavorable C_6–C_9 products with lower yields and thus can be operated at wider applied p–p voltage ranges. Catalytic dehydrogenation of hexane is the source of hydrogen. Online MS studies showed that methane was produced but at very low concentrations ($<1\%$) during hexane conversion in the PACT reactor. The power consumption of a PACT reactor is dominated by applied p–p voltage but is not obviously effected by feed space velocity. Energy efficiency will increase with decreasing residence time of feed molecules and will decrease with increasing applied p–p voltage. The greatest detected energy efficiency was achieved by nickel electrodes, with roughly 38% of the energy consumed by the PACT reactor used for cracking single carbon–carbon bonds.

Chemically inert helium was used as the carrier gas in this study to observe the reactions of *n*-hexane in the PACT reactor. Further studies using different hydrocarbon fuels and different carrier gases are planned in our laboratory.

Acknowledgments

Financial support for this research was provided by Toyota Motor Corporation and the Geosciences and Biosciences Division, Office of Basic Energy Sciences, Office of Science, U.S. Department of Energy.

References

[1] W.S. Epling, L.E. Campbell, A. Yezerets, N.W. Currier, J.E. Parks II, Catal. Rev. Sci. Eng. 46 (2) (2004) 163.
[2] T. Kanazawa, Catal. Today 96 (2004) 171.
[3] M. Takeuchi, S. Matsumoto, Top. Catal. 28 (2004) 151.
[4] S. Matsumoto, Y. Ikeda, H. Suzuki, M. Ogai, N. Miyoshi, Appl. Catal. B 25 (2000) 115.
[5] P.T. Fanson, H. Hirata, M. Ibe, S.L. Suib, S. Gomez, K. Malinger, WO 2006/083828 A2.
[6] G. Ertl, H. Knozinger, J. Weitkamp (Eds.), Handbook of Heterogeneous Catalysis, VCH, Weinheim, 1997, pp. 1955–1970, pp. 2017–2023.
[7] A. Grill, Cold Plasma in Materials Fabrication (From Fundamentals to Applications), IEEE Press, New York, 1994, pp. 46–112.
[8] X. Chen, S.L. Suib, Y. Hayashi, H. Matsumoto, J. Catal. 201 (2001) 198.
[9] S.L. Brock, M. Marquez, S.L. Suib, Y. Hayashi, H. Matsumoto, J. Catal. 180 (1998) 225.
[10] X. Chen, J. Rozak, J.-C. Lin, S.L. Suib, Y. Hayashi, H. Matsumoto, Appl. Catal. A 219 (2001) 25.
[11] F. Spiess, S.L. Suib, K. Irie, Y. Hayashi, H. Matsumoto, Catal. Today 89 (2004) 35.
[12] Y.S. Mok, Y.J. Huh, Plasma Chem. Plasma Process. 25 (6) (2005) 625.
[13] J. Luo, S.L. Suib, Y. Hayashi, H. Matsumoto, J. Phys. Chem. A 103 (1999) 6151.